Journal of Magnetic Resonance 200 (2009) 153–160

Contents lists available at ScienceDirect

Journal of Magnetic Resonance

journal homepage: www.elsevier.com/locate/jmr

Communication

Impact of selective excitation on carbon longitudinal relaxation: Towards fast solid-state NMR techniques

Mathilde Giffard [a], Michel Bardet [a], Beate Bersch [b], Jacques Covès [b], Sabine Hediger [a,*]

[a] Laboratoire de Chimie Inorganique et Biologique (UMR-E3 CEA/UJF, FRE 3200 CEA/CNRS), INAC, CEA, F-38054 Grenoble, France
[b] Institut de Biologie Structurale (UMR 5075 CEA/CNRS/UJF), 38027 Grenoble, France

ARTICLE INFO

Article history:
Received 31 March 2009
Revised 9 June 2009
Available online 13 June 2009

Keywords:
Solid-state NMR
Proteins
Longitudinal relaxation
Fast NMR
Selective pulses
Biomolecules
Spin-diffusion
Sensitivity enhancement

ABSTRACT

The effect of selective pulses on the apparent carbon longitudinal relaxation is investigated in three fully ^{13}C-labeled systems, histidine as a model system and two proteins MerP and YajG. It is shown that the longitudinal relaxation of a selectively excited carbon spin is greatly enhanced, mainly because of fast spin-diffusion. This relaxation enhancement allows reducing the time necessary for polarization recovery between two experiments. This effect can be exploited either to improve the sensitivity of NMR experiments or to reduce the experimental time. Using selective carbon excitation combined with fast pulsing on fully ^{13}C-labeled proteins, a sensitivity improvement of 20–45% over standard cross-polarization methods is predicted from the measured relaxation times.

1. Introduction

Since the first protein structure obtained by solid-state NMR in 2002 [1], the field of biomolecular solid-state NMR has expanded very quickly. The different steps of structure determination by NMR are based on a series of multidimensional (nD) NMR experiments performed on ^{13}C, ^{15}N isotopically labeled biomolecules, that allow correlating frequencies over several spectral dimensions. The major drawback of nD NMR is the long acquisition time due to the independent incrementing of time variables associated with the indirect dimensions. Several approaches have been developed in solution NMR to overcome this problem. They can be classified into two categories. The first one is based on a different way to sample the multidimensional time space. It embraces the techniques of Ultrafast NMR [2,3] proposed by Frydman and co-workers, where the entire nD acquisition is performed in one scan, projection spectroscopy [4–6], where the information of the nD spectrum is extracted from some projections of lower dimension, and non-linear sampling [7] combined with alternative processing algorithms [8–11]. The second category of techniques to fasten nD experiments consists in shortening the inter-scan delays (fast-pulsing techniques). The experimental sensitivity of such fast-pulsing techniques can be enhanced by the use of selective excitation pulses that were shown to reduce the longitudinal relaxation times [12–14]. In some cases the sensitivity for very fast repetition rates can be further reduced by Ernst-angle excitation [15], as exploited in the SOFAST experiment [16,17].

In solid-state NMR, isolated attempts to use single-scan and projection-reconstruction spectroscopy have been presented [18–20]. A broad application of these techniques is however limited due to the low sensitivity of the heteronuclei detection usually used in solid-state NMR. For the implementation of the second alternative, consisting in reducing the inter-scan delay, two limiting factors have to be taken into account: the relaxation time T_1, but also the duty cycle of the probe. Indeed, high-power pulses and decoupling used regularly in protonated solid-state samples limit the repetition rate of the experiment to the duty-cycle of the probe, usually on the order of 5%. It was demonstrated some years ago that low-power decoupling can be efficient in protonated samples if ultra-fast Magic-Angle Spinning (MAS) is used [21–23], leading recently to the first fast NMR-data acquisition on protonated samples spinning at 60 kHz [24]. Low-power experiments have the additional advantage to limit heating of the sample, especially when fast pulsing is used. The problem of the probe duty-cycle being solved, the time needed for the magnetization to recover, called in this contribution the apparent longitudinal relaxation time T_1^*, has to be fast enough to allow reduction of the repetition delay without compromising the sensitivity. Even though fast T_1^* in the order of 200–400 ms are found for protons in hydrated and protonated microcrystalline proteins, this apparent

* Corresponding author. Fax: +33 4 38 78 50 90.
E-mail address: Sabine.Hediger@cea.fr (S. Hediger).

1090-7807/$ - see front matter © 2009 Elsevier Inc. All rights reserved.
doi:10.1016/j.jmr.2009.06.008

relaxation time becomes much slower in rigid or perdeuterated samples. In this context, dilution of paramagnetic ions in the solid sample has been proposed in order to fasten the return to equilibrium of the magnetization [25–27].

Here we investigate how selective carbon pulses can significantly accelerate the carbon longitudinal relaxation. The choice of carbon spins instead of protons, as common in solution NMR was motivated by the following aspects. The strong dipolar coupling among protons leads to a strongly coupled proton system rendering the use of standard selective pulses impossible, except perhaps at much higher spinning speeds than those available in most NMR laboratories. Additionally, in fully ^{13}C-labeled samples, the number of protons per carbon spin is not high enough to obtain the maximum theoretical sensitivity gain from cross-polarization (CP), which in such samples was reported not to be necessarily much better than direct carbon excitation [28]. Improvement of the apparent longitudinal carbon relaxation may therefore render the direct excitation of carbons competitive with CP. To study the impact of selective excitation on the apparent longitudinal relaxation times of carbons, selective inversion–recovery experiments were performed on a model system, fully ^{13}C-labeled histidine, and on two fully ^{13}C-labeled proteins, MerP (72 residues) [29] and YajG (192 residues) [30]. The measurements were performed at intermediate and fast MAS frequencies, representing the two regimes where the carbon resonances are not broadened by rotational resonance effects [31–33], namely below the CO–C_α and above any other rotational resonance condition. In the selective excitation cases, the apparent mono-exponential relaxation of carbon magnetization is replaced by a strong bi-exponential behavior with a very fast component attributed to spin-diffusion from the many equilibrium carbon spins to the excited one. This fast component reduces considerably the apparent relaxation time of the selectively inverted carbon spin. On the basis of the measured relaxation time constants, curves of signal-to-noise-ratio per unit time $(S/N)_t$ were calculated as a function of the repetition time of the experiment, allowing the comparison of the sensitivity of selective carbon excitation with non-selective direct excitation and CP. Thus, for hydrated protein samples, a sensitivity improvement is predicted for selective excitation over CP at short repetition times of the pulse sequence.

2. Materials and methods

Uniformly ^{13}C-, ^{15}N-labeled L-histidine was purchased from Cambridge Isotope Laboratories and re-crystallized in a 0.9 mM $CuCl_2$ solution. After crystallization, a mixture of two different crystal forms, denoted for convenience in this contribution A- and B-histidine, was obtained in different proportions. Fig. 1 shows the ^{13}C CPMAS NMR spectrum of the histidine sample. By comparing the measured chemical shifts, we could assign the resonances of the minor form (A-histidine) and the major form (B-histidine) to the crystal structures described in Refs. [34] and [35], respectively. Carbon assignment of the histidine spectrum is given in Table 1. Almost all resonances of both crystal forms are resolved. Overlapping is only found for both C_β (A- and B-form), and for A-C_2, B-C_2 and A-C_4.

Uniformly ^{13}C-, ^{15}N-labeled MerP from *Cupriavidus metalliduran*s CH34 was produced as follows. The DNA fragment coding for the cytoplasmic part of the MerP protein (residues 20–91 of the full-length sequence) was amplified by PCR with suitable restriction sites for subcloning in the expression vector pET28a. The authenticity of the DNA insert generated by PCR was confirmed by sequencing. The resulting plasmid pET28-MerPcyt was used to transform the T7 RNA polymerase-containing host *Escherichia coli* BL21(DE3). The freshly transformed bacteria were grown at 37 °C in M9 minimal mineral medium with $^{15}NH_4Cl$ (1 g/L) and

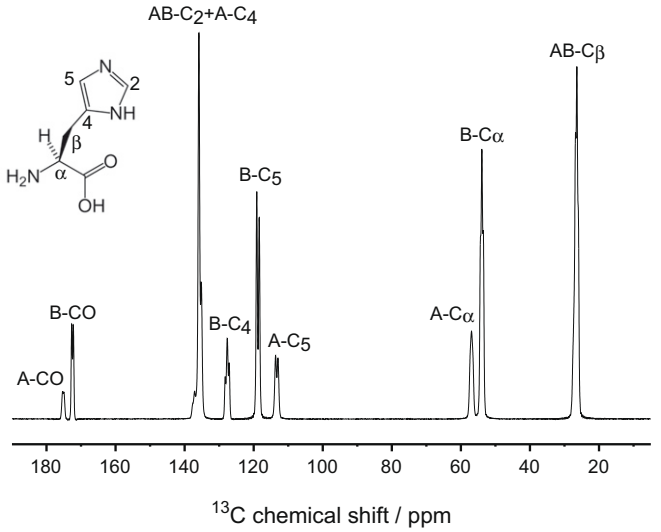

Fig. 1. NMR ^{13}C CPMAS spectrum of uniformly ^{13}C-labeled histidine. IUPAC nomenclature was used for the labeling of carbons in the histidine molecule. The two crystal forms found in the sample are arbitrarily labeled A and B.

Table 1
Experimental ^{13}C chemical-shift values of A-histidine and B-histidine.

	^{13}C chemical shift[a]/ppm					
	C=O	C_2	C_4	C_5	C_α	C_β
A-histidine[b] (minor)	175.2	135.2	137.2	113.3	57.0	26.5
B-histidine[c] (major)	172.5	135.9	127.7	118.8	53.9	26.5

[a] Chemical shift values are calibrated indirectly using the glycine carbonyl resonance set at 176.45 ppm with respect to DDS.
[b] Crystalline form described in Ref. [34].
[c] Crystalline form described in Ref. [35].

$^{13}C_6$-glucose (2 g/L) as sole nitrogen and carbon sources, and supplemented with $MnCl_2$ (0.1 mM), $ZnSO_4$ (0.05 mM), $FeCl_3$ (0.05 mM) and a vitamin solution according to Ref. [36]. Protein expression was induced by the addition of 0.5 mM isopropyl-1-thio-β-D-galactopyranoside when cells reached an A_{600} between 0.6 and 0.8. Cells were grown overnight at 20 °C and harvested by centrifugation. The protein was then purified as previously described [29]. The pure protein was concentrated up to 30 mg mL^{-1} in a Diaflow cell equipped with a YM-3 membrane (Amicon corp.). The final buffer was 50 mM Tris/HCl pH 7.5. Crystals suitable for solid-state NMR were obtained by using the sitting-drop vapor-diffusion method at 293 K as follows. Drops were prepared by mixing 20 μL of MerP with 20 μL reservoir solution composed of 40% unbuffered PEG 4000. Crystals appeared in less than 24 h when the drops were equilibrated against 1 mL reservoir solution. Crystals from 20 drops were harvested and centrifuged directly into the NMR rotor.

Fully ^{13}C–^{15}N-labeled YajG protein [30] has been provided by Dr. J.-P. Simorre from the Structural Biology Institute in Grenoble (France). The protein was slowly precipitated in water and directly centrifuged into the NMR rotor.

All solid-state NMR experiments were performed at 9.4 T (^{1}H NMR frequency of 400.13 MHz) using a Bruker 400 NMR spectrometer. For experiments at 9 kHz MAS, a Bruker 4 mm MAS double-resonance probe was used. The bearing gas temperature was set to 283 and 268 K for the histidine and MerP samples, corresponding to a sample temperature of 293 and 280 K, respectively. For the experiments at 30 kHz MAS, a Bruker double-resonance 2.5 mm

MAS probe was used. The sample temperature was stabilized at 293 K (bearing gas at 268 K) for the histidine sample and at 301 K for YajG.

The longitudinal relaxation behavior of proton and carbon spins was measured by inversion–recovery experiments. As in uniformly ^{13}C-labeled samples the relaxation of longitudinal proton or carbon magnetization is not only dictated by incoherent modulation of anisotropic interactions due to molecular dynamics, but also by multi-spin deterministic mechanisms such as spin-diffusion, we choose to call the apparent measured relaxation times T_1^* (in analogy to T_2^* used in solid-state NMR for the apparent FID decay), reserving T_1 for the relaxation induced by molecular dynamics. Proton T_1^* (T_{1H}^*) were measured indirectly on carbons, with a CP step of 1 ms (1.5 ms in experiments on YajG) after the inversion of the protons and the incremented recovery time. Experimental conditions for CP were not optimized individually for each resonance, but set to the best compromise in terms of sensitivity for the entire spectrum. Carbon T_1^* (T_{1C}^*) were measured by a standard inversion–recovery experiment applied directly on carbons. This was preferred to the method of Torchia [37] which leads to exponential decaying curves, but requires a CP transfer from protons to carbons. In case of a non-uniform polarization of the different carbon spins after CP, the beginning of the decaying curves measured with Torchia's method are perturbed by spin-diffusion effects among the different carbons. This effect is avoided with the standard inversion–recovery experiment. In the non-selective carbon inversion–recovery experiment, a τ–π–τ echo period in presence of ^{1}H decoupling was added prior to detection to avoid background signal from the probe. The echo time τ was set to one rotor period. For the selective T_{1C}^* measurements, a selective 180° I-Burp1 pulse [38,39] was used to invert the desired ^{13}C spin followed by the incremented recovery time and a hard 90° detection pulse. The length of the selective pulse (between 620 μs and 2 ms) was adjusted to invert selectively each resonance type of the histidine sample (CO, C_α or aromatic signals). For the protein samples, the selective inversion pulse was designed in such a way that it acted separately on the CO, C_α or $C_{\beta-\delta}$ region. ^{1}H heteronuclear decoupling was applied during the selective 180° pulse. The carbon rf-field strength was 60 kHz for all hard pulses. SPINAL heteronuclear decoupling [40] at a rf-field strength of 90 kHz (9 kHz MAS) or 120 kHz (30 kHz MAS) was applied during detection in all experiments. For the experiments at 9 kHz MAS, the acquisition time was set to 30 ms for histidine and 20 ms for MerP. It was set to 45 and 20 ms for experiments at 30 kHz MAS on histidine and YajG, respectively. The repetition delay was adjusted such that it was always longer than 6 times the slowest measured T_1^* component.

The apparent relaxation times T_1^* (T_{1H}^* or T_{1C}^*) were extracted from the inversion–recovery curves by fitting the signal intensity or integral $I(t)$ as a function of the recovery time t to a multi-exponential function of the form:

$$I(t) = I_0\left(1 - A\sum_{n=1}^{i} B_n \exp\left\{-\frac{t}{T_{1,n}^*}\right\}\right), \quad \text{with}\sum_{n=1}^{i} B_n = 1 \tag{1}$$

where A is the inversion quality factor ($A \sim 2$), and the factors B_n are the normalized weights of the different exponential components. All ^{1}H and non-selective ^{13}C relaxation curves could be fitted with a mono-exponential equation ($i = 1$), except for one aromatic and the C_β carbon resonances, which contain signal from both crystalline forms of histidine ($i = 2$). All selective ^{13}C relaxation curves required two components to be fitted.

Using the measured T_1^* time constants, theoretical curves of signal-to-noise ratio per unit time $(S/N)_t$ as a function of the experimental time T_{scan} were calculated using the following equation [17]:

$$(S/N)_t = \eta\frac{1 - \sum_{n}^{i} B_n \exp\left\{-\frac{T_{\text{rec}}}{T_{1,n}^*}\right\}}{\sqrt{T_{\text{scan}}}} \tag{2}$$

The experimental time T_{scan} is defined as the total time needed for one transient (scan) of the experiment, e.g. the sum of the inter-scan delay, the pulse-sequence duration and the acquisition time. The recycle time T_{rec} comprises only the time intervals where the spins relax back towards equilibrium after the pulse sequence. For non-selective experiments, T_{rec} is thus given by the sum of inter-scan delay and acquisition time. In selective experiments, two components contribute to the relaxation. The fast component, which is attributed to spin-diffusion, becomes only active once the proton decoupling stops. For this fast component, only the interscan delay was taken into account for T_{rec}. For the slow component, T_{rec} is the same as in non-selective experiments. B_n are the normalized factors obtained from Eq. (1). The enhancement factor η takes into account the sensitivity enhancement of CP over direct ^{13}C excitation. It is set to 1 for direct broadband or selective excitation, and should reach about 2.4 for CP experiment in fully labeled proteins or amino acids [28].

NMR data were processed with Topspin2.0 software, and the relaxation curves were fitted with Origin7.5.

3. Results and discussion

3.1. Histidine sample

First, we have measured non-selective longitudinal relaxation times of protons T_{1H}^* and carbons T_{1C}^* for histidine at 9 kHz MAS. All resolved carbon resonances show a mono-exponential behavior for the inversion–recovery curves (not shown). As expected, the measured time constants T_{1H}^* or T_{1C}^* are very similar for resonances originating from the same crystalline form of histidine, as spin-diffusion among protons as well as among carbons averages the relaxation times over the molecule. Interestingly, the apparent longitudinal relaxation times are faster for the A-form, about 0.7 and 30 s for T_{1H}^* and T_{1C}^*, respectively, compared to 3.6 and 84 s for the B-form. We believe that this difference is explained by the co-crystallization of paramagnetic Cu^{2+} ions inside A-histidine only. This explains also the slightly lower resolution obtained for the resonances of A-histidine compared to B-histidine (see Fig. 1). Considering the difference of more than one order of magnitude between the relaxation times of ^{1}H and ^{13}C, it is evident that CP techniques are much more efficient than direct broadband ^{13}C excitation for rigid solids, as they allow a faster repetition rate of the experiment without compromising sensitivity.

Interestingly, selective inversion of one ^{13}C resonance leads to a significantly different longitudinal relaxation behavior compared to broadband inversion. As an example, the recovery curve of the B-histidine CO resonance after its selective inversion is shown in Fig. 2a). This selective recovery curve is representative of all other resonances in histidine when selectively inverted. Return to equilibrium after selective inversion is clearly bi-exponential, with a very fast component of about 1–20 ms depending on the inverted resonance (exact values are given in Table 2). This fast component is important as it brings back about 70–80% of the equilibrium magnetization. The mechanism for this fast recovery component is attributed to proton-driven spin-diffusion. Indeed, as only one carbon spin is inverted, a difference of polarization is created between the inverted spin and its neighbors. Zero-quantum proton-driven spin-diffusion will act on this polarization difference during the recovery time to re-equilibrate the total polarization on all carbon spins. This effect has been already observed a long time ago in natural abundance ^{13}C polymers by VanderHart [41]. As expected, the re-equilibration of polarization

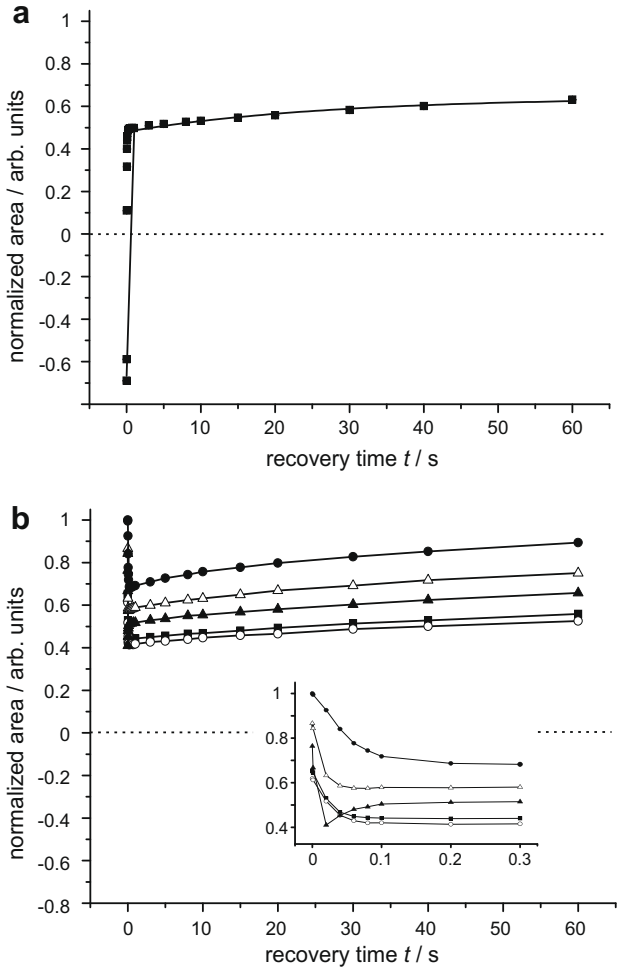

Fig. 2. ^{13}C-magnetization recovery curves after selective inversion of the B-CO resonance of histidine at 9 kHz MAS for (a) the excited B-CO resonance (filled squares), and (b) the non-excited B-C_α (filled triangles), B-C_β (open triangles), B-C_4 (filled squares), B-C_5 (open circles), and B-C_2 (filled circles) resonances. In (a) the solid line is a bi-exponential fit to the experimental data according to Eq. (1). In (b) the insert shows an expansion of the data for short recovery times, and the lines are smoothened interpolations of the experimental data points.

Table 2
Fast selective T_{1C}^* component in ms for different resonances of Histidine

	A-CO	B-CO	B-C_4	B-C_5	A-C_α	B-C_α	AB-C_β
9 kHz MAS	20.9	19.1	1.5	2.2	8.1	6.6	2.7
30 kHz MAS	3936	11,007	34.2	41.0	63.1	41.4	46.6

is also visible for the non-inverted resonances of histidine, which all show a fast decrease of their longitudinal magnetization before recovering to equilibrium (see Fig. 2b). The time scale of this decrease is about the same as the fast recovery component of the inverted resonance, and corresponds also to the build-up time constant of cross-peaks in a 2D proton-driven spin-diffusion experiment (not shown).

Values of the second, slower recovery component after selective inversion are compared to non-selective T_{1C}^* in Fig. 3(a) for different resonances of histidine. Interestingly, even the slow component of the selective T_{1C}^* is significantly faster than the broadband T_{1C}^* for all measured resonances. It remains however slower than T_{1H}^* (see Fig. 3a). The physical mechanism leading to this enhanced recovery of magnetization after re-equilibration of polarization by spin-diffusion is still unclear, but could be attributed to long-range spin-diffusion effects.

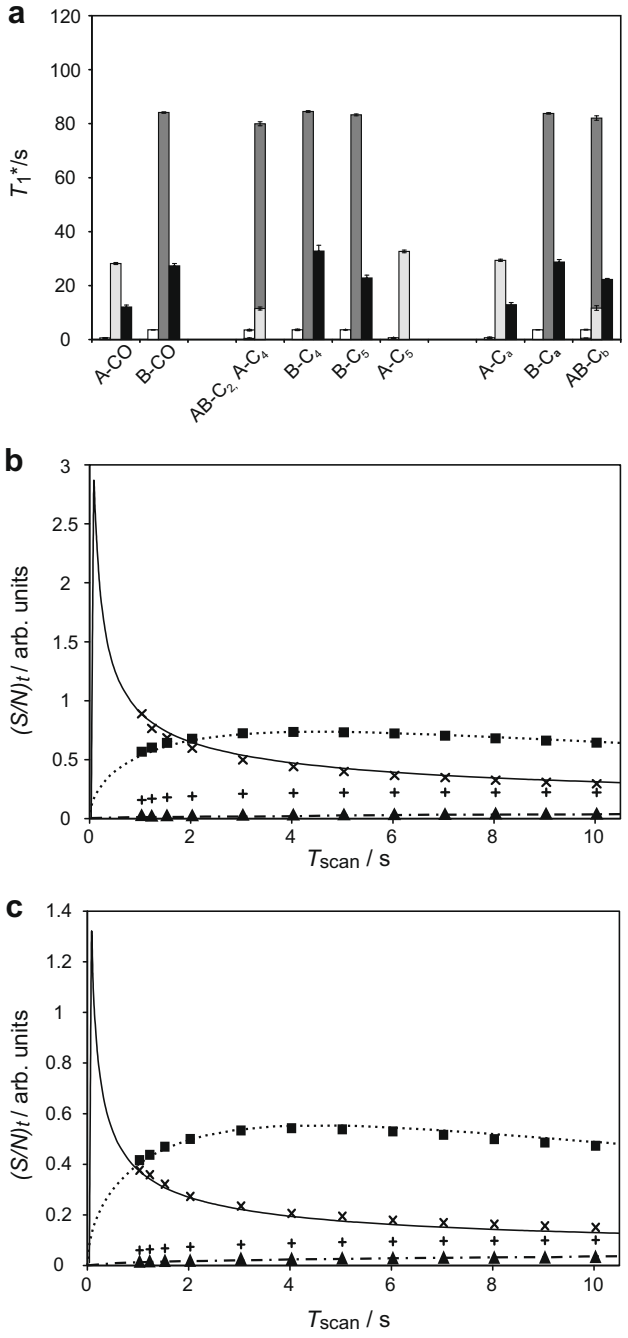

Fig. 3. (a) T_1^* values measured for histidine from inversion–recovery experiments at 9 kHz MAS using CPMAS (T_{1H}^*, white bars), broadband carbon excitation (T_{1C}^*, light and dark grey bars for A- and B-histidine, respectively), and selective carbon excitation (T_{1C}^*, black bars). For the selective T_{1C}^*, only the slow component of the bi-exponential curve is represented. Error bars indicate standard errors in the experimental determination of the time constants. (b and c) Calculated and experimental $(S/N)_t$ plotted as a function of the scan time T_{scan} for (b) B-CO and (c) B-C_α resonances of histidine at 9 kHz MAS. Lines are numerical curves calculated with Eq. (2) for CPMAS (dotted lines), direct excitation (dashed lines), and selective excitation (solid lines), using the experimental T_1^* values given in (a). The CP enhancement factor η used to calculate the $(S/N)_t$ of CP (dotted line) was adjusted in such a way to best fit the experimental points. It was set to 2.2 in (b) and 1.65 in (c). Theoretical curves are compared to experimental points obtained using CPMAS (filled squares), direct excitation (filled triangles), and selective excitation (crosses and plus signs). For each experimental point, the signal was accumulated over 8 scans after 32 dummy scans, except for points labeled with crosses where only 2 scans after 2 dummy scans were used.

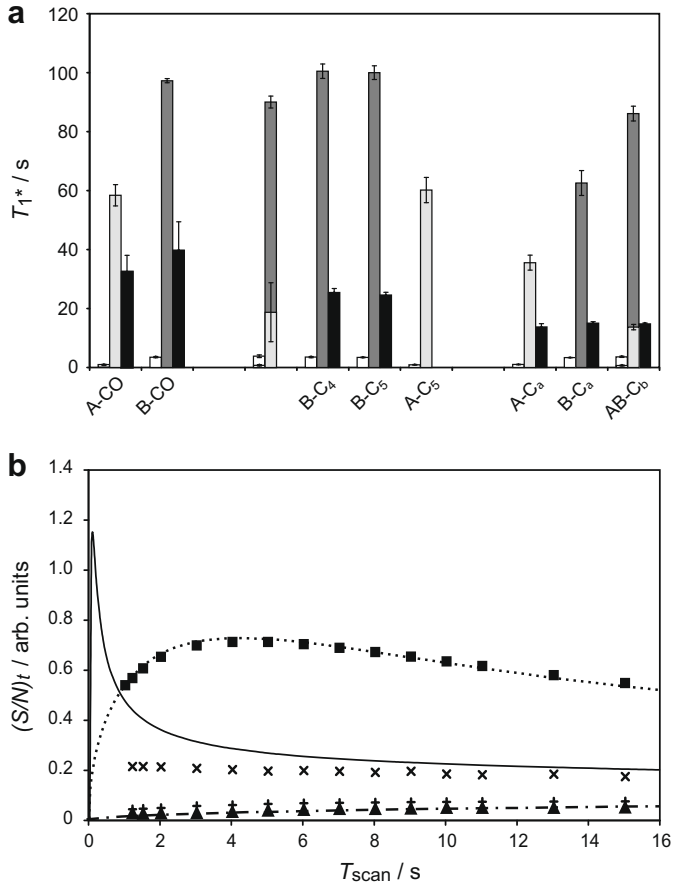

Fig. 4. (a) T_1^* values measured for histidine from inversion–recovery experiments at 30 kHz MAS using CPMAS (white bars), broadband carbon excitation (light and dark grey bars for A- and B-histidine, respectively), and selective excitation (black bars). For the selective T_{1C}^*, only the slow component of the bi-exponential curve is represented (black bars). (b) Calculated and experimental $(S/N)_t$ plotted as a function of the scan time T_{scan} for the B-C_α resonance of histidine at 30 kHz MAS. Lines are numerical curves calculated with Eq. (2) for CPMAS (dotted lines), direct excitation (dashed lines), and selective excitation (solid lines) using the experimental T_1^* values given in (a). The enhancement factor η for the CPMAS curve was adjusted to best fit the experimental points ($\eta = 2.1$). Experimental points were obtained using CPMAS (filled squares), direct excitation (filled triangles), and selective excitation (black crosses and plus signs), using 64 scans after 32 dummy scans, except for points labeled with crosses (2 dummy scans and 2 scans).

In order to estimate whether experiments based on selective carbon excitation can compete with CP-based techniques, theoretical curves of signal-to-noise-ratio per unit time $(S/N)_t$ were calculated using Eq. (2) for CP, broadband and selective ^{13}C excitation. The curves are compared in Fig. 3(b) and (c) for B-CO and B-C_α resonances of histidine, respectively, together with a few experimental points. The experimental points agree very well with the

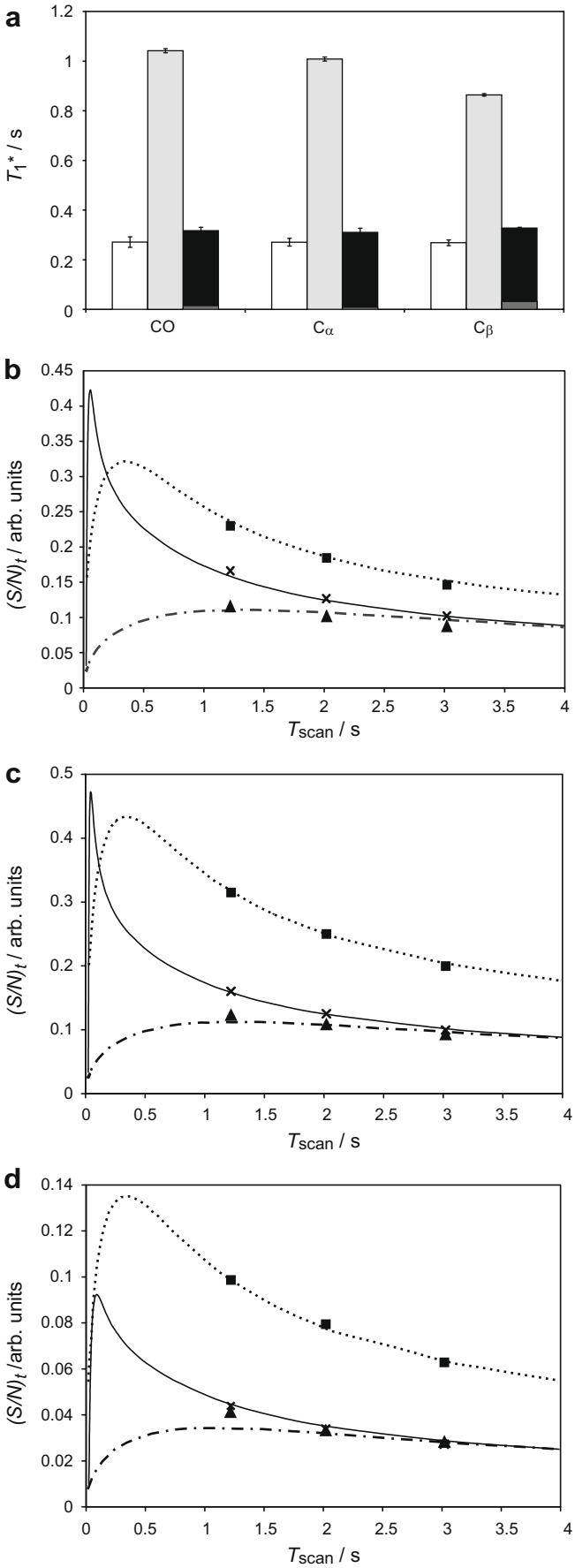

Fig. 5. (a) T_1^* values measured for fully ^{13}C-labeled MerP from inversion–recovery experiments at 9 kHz MAS using CPMAS (white bars), broadband carbon excitation (light grey bars), and selective excitation (dark-grey and black bars for the fast and the slow components, respectively). The inversion–recovery curves were obtained by integrating separately over the CO, C_α, and $C_{\beta-\delta}$ regions of the spectrum. (b–d) Calculated and experimental $(S/N)_t$ plotted as a function of T_{scan} for (b) the CO, (c) the C_α, and (d) the $C_{\beta-\delta}$ regions of MerP at 9 kHz MAS. Lines are numerical curves calculated with Eq. (2) for CPMAS (dotted lines), direct excitation (dashed lines), and selective excitation (solid lines), using the experimental T_1^* given in (a). The enhancement factor η for the CPMAS curve was adjusted to best fit the CP experimental points. It was set to 1.5, 2.0, and 2.2 in (b–d), respectively. Experimental points were obtained using CPMAS (filled squares), direct excitation (filled triangles), and selective excitation (black crosses), accumulating 512 scans after 8 dummy scans for each point.

simulated recovery curves. Theoretically, optimal sensitivity is obtained with selective excitation at short inter-scan delay (T_{scan} < 1 s). This could only be verified experimentally when very few transients (scans) are accumulated (see experimental points with symbol × acquired using 2 dummy scans followed by 2 real scans in Fig. 3(b) and (c)). When more dummy scans are used to reach steady-state conditions (see experimental points with symbol + acquired after 32 dummy scans), sensitivity is lost at short T_{scan}, as a result of a slow depolarization of the non-excited coupled carbon spins (called in the following carbon bath). Indeed, after a first experimental scan, some polarization from the equilibrium carbon spins is transferred to the excited one, which allows its faster recovery. When the repetition rate is faster than the longitudinal relaxation of the non-excited spins, a depolarization of the carbon bath is observed. The spin-diffusion contribution to selective T^*_{1C} is consequently decreased, and the overall sensitivity is reduced. Selective excitation can therefore only compete with CP at short inter-scan delays, if the non-excited carbon bath is large enough and relaxes in a time comparable to the repetition delay of the experiment.

As very fast repetition rates are for the moment only conceivable when combined with low-power sequences (as required from the probe duty cycle), and therefore at very high MAS spinning speed, the inversion–recovery experiments were repeated at 30 kHz MAS on histidine. In this regime again, the apparent relaxation behavior after CP (T^*_{1H}) or broadband carbon inversion (T^*_{1C}) was found to be mono-exponential, with an average T^*_{1H} of 0.9 and 3.4 s for A- and B-histidine, respectively, and 60 s (A-histidine) and 99 s (B-histidine) for non-selective T^*_{1C} (see Fig. 4(a)). Stronger variations around the average values were observed compared to the previous experiments at 9 kHz as a result of a better averaging of dipolar couplings at 30 kHz MAS. Notably, there is a strong increase in T^*_{1C} of the A-form, probably due to a better averaging of the dipolar coupling to the electronic spin of the paramagnetic Cu^{2+} ion, which becomes then less efficient as a relaxing agent.

After selective inversion, the recovery of carbon polarization is qualitatively the same as at 9 kHz MAS, with a fast and a slow relaxing component. The fast component is however much slower than at 9 kHz MAS (see Table 2), especially for the CO resonances. It is also observed that only carbon spins with a chemical shift close to the one of the inverted spin contribute to the spin-diffusion mechanism allowing for fast recovery of the inverted carbon-spin magnetization. Polarization transfer from other spins happens as well, but on a longer time scale. These observations are all in good agreement with what is expected from spin-diffusion at high spinning speed. However, even at 30 kHz MAS the slow recovery component after selective inversion is much faster that the non-selective T^*_{1C} (see Fig. 4(a)).

In Fig. 4(b), theoretical curves of signal-to-noise ratio per unit time $(S/N)_t$ calculated with the measured T^*_1 of B-C_α resonance and Eq. (2) are compared for CP, broadband and selective ^{13}C excitation at 30 kHz MAS. Despite the slower spin-diffusion, selective excitation becomes theoretically more efficient than CP at fast repetition rates of the experiment (T_{scan} < 1 s). Experimentally however, the carbon bath around the selective excited spin has become too small as a result of better averaging of dipolar couplings

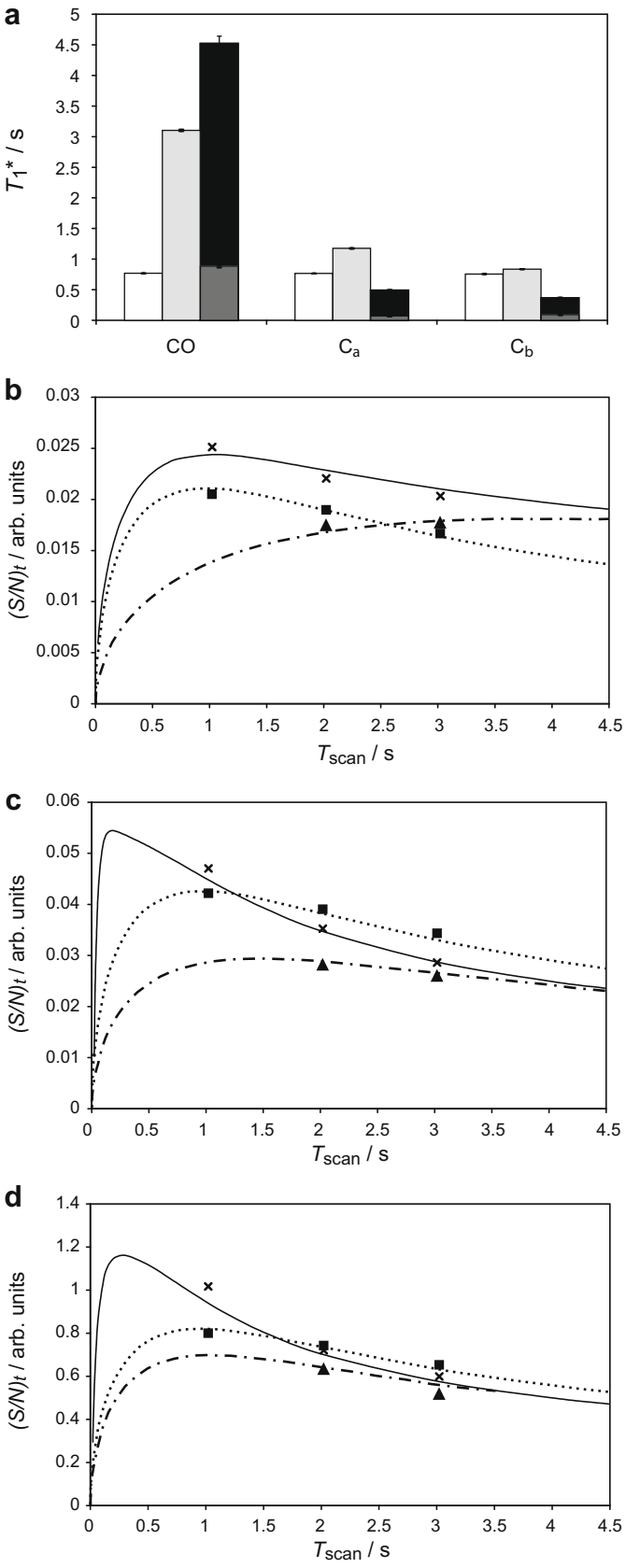

Fig. 6. (a) T^*_1 values measured for fully ^{13}C-labeled YajG from inversion–recovery experiments at 30 kHz MAS using CPMAS (white bars), broadband carbon excitation (light grey bars), and selective excitation (dark-grey and black bars for the fast and the slow components, respectively). The inversion–recovery curves were obtained by integrating separately over the CO, C_α, and $C_{\beta-\delta}$ regions of the spectrum. (b–d) Calculated and experimental $(S/N)_t$ plotted as a function of T_{scan} for (b) the CO, (c) the C_α, and (d) the $C_{\beta-\delta}$ regions of YajG at 30 kHz MAS. Lines are numerical curves calculated with Eq. (2) for CPMAS (dotted lines), direct excitation (dashed lines), and selective excitation (solid lines), using the experimental T^*_1 values given in (a). The enhancement factor η for the CPMAS line was adjusted to best fit the experimental points. It was set to 0.58, 1.17, and 1.12 in (b–d), respectively. Experimental points were obtained using CPMAS (filled squares), direct excitation (filled triangles), and selective excitation (black crosses), accumulating 400 scans after 8 dummy scans for each point.

at such high spinning speed, and even with very few transients, a depolarization of the coupled equilibrium spins is observed leading to a loss of sensitivity compared to the theoretical expectation. The behavior of aromatic resonances (not shown) is similar to the B-C_α resonance. For the carbonyl resonances, spin-diffusion is getting so slow that even at fast repetition rates of the experiment, selective excitation cannot compete with CP (data not shown).

Our results on histidine suggest that despite the enhancement of the apparent carbon relaxation obtained by the use of selective excitation of carbon spins, this approach does not seem very promising for designing fast NMR sequences for crystalline solids. Indeed, even if a significant sensitivity improvement is predicted by using selective carbon excitation combined with very fast repetition rates of the experiment, depolarization of the carbon bath will appear in the course of the experiment as a result of the slow relaxation times of carbon spins. Nevertheless, much faster carbon relaxation rates are found in hydrated solid-state biomolecular samples. Consequently, the selective excitation approach may be interesting to fasten experiments in biomolecular solid-state NMR. To test this hypothesis, we have investigated the sensitivity of selective carbon excitation for two protein samples.

3.2. Solid-state protein samples

As mentioned above, T^*_{1H} as well as non-selective T^*_{1C} time constants measured on hydrated MerP and YajG are much faster than what has been measured for crystalline histidine both at 9 kHz (Fig. 5a) and 30 kHz MAS (Fig. 6a). At 9 kHz MAS, T^*_{1H} values in MerP are around 270 ms. They are lengthened to about 760 ms in YajG when spinning at 30 kHz. Non-selective T^*_{1C} values are about 1 s, both at 9 and 30 kHz, except for the CO resonances that show a longer time constant of ~3 s at the higher spinning speed. The selective ^{13}C recovery curves present a similar behavior as described above for histidine, with a very fast component coming from spin-diffusion and a slower component. The time constants of the fast spin-diffusion component (see Figs. 5 and 6a) are similar for MerP and YajG to the ones of histidine at the corresponding spinning speed (Table 2). For MerP at 9 kHz MAS, the slower components of the selective T^*_{1C} show values which are close to T^*_{1H}. This is however not enough to counterbalance the polarization enhancement of CP. As shown in Fig. 5(b–d), better sensitivity is found with selective excitation only at very short inter-scan delays (T_{scan} < 200 ms), if at all.

In YajG at 30 kHz MAS, the selective T^*_{1C} recovery is globally faster than the ^1H one, except for CO resonances (Fig. 6a). Additionally, CP transfer under these conditions of spinning speed and rf fields was found to be very inefficient, resulting in an enhancement factor η as low as 1.1 for C_α and $C_{\beta-\delta}$ resonances. For the CO region, a better sensitivity can be obtained at longer CP contact times, but at the cost of the rest of the spectrum. In such conditions, selective excitation becomes attractive in terms of sensitivity. Indeed, as shown in Fig. 6(b–d), the sensitivity of selective carbon excitation is better than CP for all resonance types in YajG for recycle times shorter than 1.5 s, with an optimum for $T_{scan} \sim 200–300$ ms. Due to the globally fast proton and carbon relaxation in hydrated protein samples, depolarization of the equilibrium carbon spins in selective experiments were neither observed for MerP nor for YajG at repetition times as short as 1 s.

4. Conclusions

We have demonstrated that the use of selective carbon excitation in fully ^{13}C-labeled samples leads to a significant enhancement of the apparent longitudinal relaxation of the excited spin. This enhancement comes to a large part from a spin-diffusion process between the non-excited carbons in equilibrium and the selectively excited one. Spin-diffusion occurs on a time scale shorter than 100 ms. Despite the better averaging of dipolar couplings at high MAS spinning speed, which is expected to quench spin-diffusion, the enhancement of longitudinal relaxation was still important at spinning speeds as fast as 30 kHz. The apparent magnetization recovery observed after selective carbon excitation is fast enough to compete with CP at short repetition times of the experiment. In crystalline solids, the theoretical gain in sensitivity could however not be obtained experimentally, because of a depolarization of the equilibrium carbon bath for repetition rates of the experiment much shorter than the non-selective carbon longitudinal relaxation times. This drawback seems not to be present for hydrated labeled protein samples with much faster longitudinal relaxation. Thus, based on the measured relaxation times of the protein YajG at 30 kHz MAS, a sensitivity enhancement of 20–45% is predicted for selective excitation compared to optimal CP sensitivity when the repetition time is set to 200–300 ms. The relaxation enhancement obtained by selective carbon excitation may become of interest for the development of fast NMR methods in biomolecular solid-state NMR.

Acknowledgment

The authors thank Dr. J.P. Simorre from Institute of Structural Biology in Grenoble for the generous gift of YajG sample.

References

[1] F. Castellani, B. van Rossum, A. Diehl, M. Schubert, K. Rehbein, H. Oschkinat, Structure of a protein determined by solid-state magic-angle-spinning NMR spectroscopy, Nature 420 (2002) 98–102.
[2] L. Frydman, A. Lupulescu, T. Scherf, Principles and features of single-scan two-dimensional NMR spectroscopy, J. Am. Chem. Soc. 125 (2003) 9204–9217.
[3] L. Frydman, T. Scherf, A. Lupulescu, The acquisition of multidimensional NMR spectra within a single scan, Proc. Natl. Acad. Sci. USA 99 (2002) 15858–15862.
[4] E. Kupce, R. Freeman, Reconstruction of the three-dimensional NMR spectrum of a protein from a set of plane projections, J. Biomol. NMR 27 (2003) 383–387.
[5] E. Kupce, R. Freeman, Projection-reconstruction technique for speeding up multidimensional NMR spectroscopy, J. Am. Chem. Soc. 126 (2004) 6429–6440.
[6] M. Mishkovsky, E. Kupce, L. Frydman, Ultrafast-based projection-reconstruction three-dimensional nuclear magnetic resonance spectroscopy, J. Chem. Phys. 127 (2007) 034507.
[7] D. Marion, Fast acquisition of NMR spectra using Fourier transform of non-equispaced data, J. Biomol. NMR 32 (2005) 141–150.
[8] J.C. Hoch, A.S. Stern, Nucl, Mag. Reson. Biol. Macromol. Pt A 338 (2001) 159–178.
[9] K. Kazimierczuk, W. Kozminski, I. Zhukov, Two-dimensional Fourier transform of arbitrarily sampled NMR data sets, J. Magn. Reson. 179 (2006) 323–328.
[10] V.A. Mandelshtam, FDM: the filter diagonalization method for data processing in NMR experiments, Prog. Nucl. Magn. Reson. Spectrosc. 38 (2001) 159–196.
[11] V.Y. Orekhov, I. Ibraghimov, M. Billeter, Optimizing resolution in multidimensional NMR by three-way decomposition, J. Biomol. NMR 27 (2003) 165–173.
[12] K. Pervushin, B. Vogeli, A. Eletsky, Longitudinal ^1H relaxation optimization in TROSY NMR spectroscopy, J. Am. Chem. Soc. 124 (2002) 12898–12902.
[13] P. Schanda, H. Van Melckebeke, B. Brutscher, Speeding up three-dimensional protein NMR experiments to a few minutes, J. Am. Chem. Soc. 128 (2006) 9042–9043.
[14] E. Lescop, P. Schanda, B. Brutscher, A set of BEST triple-resonance experiments for time-optimized protein resonance assignment, J. Magn. Reson. 187 (2007) 163–169.
[15] R.R. Ernst, G. Bodenhausen, A. Wokaun, Principles of Nuclear Magnetic Resonance in One and Two Dimensions, Oxford University Press Inc., New York, 1987.
[16] P. Schanda, B. Brutscher, Very fast two-dimensional NMR spectroscopy for real-time investigation of dynamic events in proteins on the time scale of seconds, J. Am. Chem. Soc. 127 (2005) 8014–8015.
[17] P. Schanda, E. Kupce, B. Brutscher, SOFAST-HMQC experiments for recording two-dimensional heteronuclear correlation spectra of proteins within a few seconds, J. Biomol. NMR 33 (2005) 199–211.
[18] M. Gal, C. Melian, D.E. Demco, B. Blumich, L. Frydman, Solid-state single-scan 2D NMR under magic-angle-spinning, Chem. Phys. Lett. 459 (2008) 188–193.
[19] K. Bertelsen, J.M. Pedersen, N.C. Nielsen, T. Vosegaard, 2D separated-local-field spectra from projections of 1D experiments, J. Magn. Reson. 184 (2007) 330–336.

[20] T. Vosegaard, D. Massiot, High-resolution two-dimensional NMR spectra of half-integer-spin quadripolar nuclei from one-dimensional projections, Chem. Phys. Lett. 437 (2007) 120–125.
[21] M. Kotecha, N.P. Wickramasinghe, Y. Ishii, Efficient low-power heteronuclear decoupling in ^{13}C high-resolution solid-state NMR under fast magic angle spinning, Magn. Reson. Chem. 45 (2007) S221–S230.
[22] M. Ernst, A. Samoson, B.H. Meier, Low-power XiX decoupling in MAS NMR experiments, J. Magn. Reson. 163 (2003) 332–339.
[23] M. Ernst, Heteronuclear spin decoupling in solid-state NMR under magic-angle sample spinning, J. Magn. Reson. 162 (2003) 1–34.
[24] S. Laage, J.R. Sachleben, S. Steuernagel, R. Pierattelli, G. Pintacuda, L. Emsley, Fast acquisition of multi-dimensional spectra in solid-state NMR enabled by ultra-fast MAS, J. Magn. Reson. 196 (2009) 133–141.
[25] N.P. Wickramasinghe, M. Kotecha, A. Samoson, J. Past, Y. Ishii, Sensitivity enhancement in ^{13}C solid-state NMR of protein microcrystals by use of paramagnetic metal ions for optimizing ^{1}H T_1 relaxation, J. Magn. Reson. 184 (2007) 350–356.
[26] R. Linser, V. Chevelkov, A. Diehl, B. Reif, Sensitivity enhancement using paramagnetic relaxation in MAS solid-state NMR of perdeuterated proteins, J. Magn. Reson. 189 (2007) 209–216.
[27] N.P. Wickramasinghe, S. Parthasarathy, C.R. Jones, C. Bhardwaj, F. Long, M. Kotecha, S. Mehboob, L.W.-M. Fung, J. Past, A. Samoson, Y. Ishii, Nanomole-scale protein solid-state NMR by breaking intrinsic ^{1}H T_1 boundaries, Nature Methods Advance online publication, 2009.
[28] E. Katoh, K. Takegoshi, T. Terao, ^{13}C nuclear overhauser polarization-magic-angle spinning nuclear magnetic resonance spectroscopy in uniformly ^{13}C-labeled solid proteins, J. Am. Chem. Soc. 126 (2004) 3653–3657.
[29] L. Serre, E. Rossy, E. Pebay-Peyroula, C. Cohen-Addad, J. Coves, Crystal structure of the oxidized form of the periplasmic mercury-binding protein MerP from Ralstonia metallidurans CH34, J. Mol. Biol. 339 (2004) 161–171.
[30] J. Boudet, A. Chouquet, A. Chahboune, C. Giustini, B. Joris, J.P. Simorre, C. Bougault, ^{1}H, ^{13}C and ^{15}N resonance assignments of YajG, an *Escherichia coli* protein of unknown structure and function, Biomol. NMR Assignments 1 (2007) 89–91.
[31] T. Nakai, C.A. McDowell, Calculation of rotational resonance NMR spectra using Floquet theory combined with perturbation treatment, Mol. Phys. 88 (1996) 1263–1275.
[32] D.P. Raleigh, M.H. Levitt, R.G. Griffin, Rotational resonance in solid-state NMR, Chem. Phys. Lett. 146 (1988) 71–76.
[33] A.E. Bennett, R.G. Griffin, S. Vega, in: P. Diehl, E. Fluck, R. Kosfeld (Eds.), NMR Basic Principles and Progress, Springer, Berlin, 1994, p. 1.
[34] H. Kimura, K. Nakamura, A. Eguchi, H. Sugisawa, K. Deguchi, K. Ebisawa, E. Suzuki, A. Shoji, Structural study of alpha-amino-acid crystals by ^{1}H CRAMPS NMR spectroscopy, J. Mol. Struct. 447 (1998) 247–255.
[35] C.H. Ye, R.Q. Fu, J.Z. Hu, L. Hou, S.W. Ding, ^{13}C chemical-shift anisotropies of solid amino-acids, Magn. Reson. Chem. 31 (1993) 699–704.
[36] M. Jansson, Y.C. Li, L. Jendeberg, S. Anderson, G.T. Montelione, B. Nilsson, High-level production of uniformly ^{15}N- and ^{13}C-enriched fusion proteins in *Escherichia coli*, J. Biomol. NMR 7 (1996) 131–141.
[37] D.A. Torchia, Measurement of proton-enhanced ^{13}C T_1 values by a method which suppresses artifacts, J. Magn. Reson. 30 (1978) 613–616.
[38] R. Freeman, Shaped radiofrequency pulses in high resolution NMR, Prog. Nucl. Magn. Reson. Spectrosc. 32 (1998) 59–106.
[39] H. Geen, R. Freeman, Band-selective radiofrequency pulses, J. Magn. Reson. 93 (1991) 93–141.
[40] B.M. Fung, A.K. Khitrin, K. Ermolaev, An improved broadband decoupling sequence for liquid crystals and solids, J. Magn. Reson. 142 (2000) 97–101.
[41] D.L. Vanderhart, Natural-abundance ^{13}C–^{13}C spin exchange in rigid crystalline organic-solids, J. Magn. Reson. 72 (1987) 13–47.